

Search for solar axion emission from ${}^7\text{Li}$ and $\text{D}(p, \gamma){}^3\text{He}$ nuclear decays with the CAST γ -ray calorimeter

S. Andriamonje,¹ S. Aune,¹ D. Autiero,² K. Barth,² A. Belov,³ B. Beltrán,⁴ H. Bräuninger,⁵ J. M. Carmona,⁴ S. Cebrián,⁴ J. I. Collar,⁶ T. Dafni,^{1,7} M. Davenport,² L. Di. Lella,² C. Eleftheriadis,⁸ J. Englhauser,⁵ G. Fanourakis,⁹ E. Ferrer. Ribas,¹ H. Fischer,¹⁰ J. Franz,¹⁰ P. Friedrich,⁵ T. Gerasis,⁹ I. Giomataris,¹ S. Gninenko,³ H. Gómez,⁴ M. Hasinoff,¹¹ F. H. Heinsius,¹⁰ D. H. H. Hoffmann,⁷ I. G. Irastorza,^{1,4} J. Jacoby,¹² K. Jakovčić,¹³ D. Kang,¹⁰ K. Königsman,¹⁰ R. Kotthaus,¹⁴ M. Krčmar,¹³ K. Kousouris,⁹ M. Kuster,^{5,7} B. Lakić,¹³ C. Lasseur,² A. Liolios,⁸ A. Ljubičić,¹³ G. Lutz,¹⁴ G. Luzón,⁴ D. W. Miller,^{4,*} J. Morales,⁴ A. Ortiz,⁴ T. Papaevangelou,² A. Placci,² G. Raffelt,¹⁴ H. Riege,⁷ A. Rodríguez,⁴ J. Ruz,⁴ I. Savvidis,⁸ Y. Semertzidis,¹⁵ P. Serpico,¹⁶ L. Stewart,² J. D. Vieira,⁶ J. Villar,⁴ J. Vogel,¹⁰ L. Walckiers,² and K. Zioutas²

¹DAPNIA, Centre d'Études Nucléaires de Saclay, Gif-sur-Yvette, France

²European Organization for Nuclear Research (CERN), CH-1211 Genève 23, Switzerland[†]

³Institute for Nuclear Research, Russian Academy of Sciences, Moscow, Russia

⁴Instituto de Física Nuclear y Altas Energías, Universidad de Zaragoza, Zaragoza, Spain[‡]

⁵Max-Planck-Institut für extraterrestrische Physik, Geissenbachstrasse, 85748 Garching, Germany

⁶Enrico Fermi Institute and KICP, University of Chicago, Chicago, IL, USA

⁷Technische Universität Darmstadt, Institut für Kernphysik, Schlossgartenstrasse 9, 64289 Darmstadt, Germany[§]

⁸Aristotle University of Thessaloniki, Thessaloniki, Greece

⁹National Center for Scientific Research "Demokritos", Athens, Greece

¹⁰Albert-Ludwigs-Universität Freiburg, Freiburg, Germany

¹¹Department of Physics and Astronomy, University of British Columbia, Vancouver, Canada

¹²Johann Wolfgang Goethe-Universität, Institut für Angewandte Physik, Frankfurt am Main, Germany

¹³Rudjer Bošković Institute, Bijenička cesta 54, P.O.Box 180, HR-10002 Zagreb, Croatia

¹⁴Max-Planck-Institut für Physik (Werner-Heisenberg-Institut), Föhringer Ring 6, 80805 München, Germany

¹⁵University of Patras, Patras, Greece[¶]

¹⁶Particle Astrophysics Center - Fermi National Accelerator Laboratory, Batavia, IL 60510, USA

(Dated: May 8, 2022)

We present the results of a search for a high-energy axion emission signal from ${}^7\text{Li}$ (0.478 MeV) and $\text{D}(p, \gamma){}^3\text{He}$ (5.5 MeV) nuclear transitions using a low-background γ -ray calorimeter during Phase I of the CAST experiment. These so-called "hadronic axions" could provide a solution to the long-standing *strong-CP* problem and can be emitted from the solar core from nuclear M1 transitions. This is the first such search for high-energy pseudoscalar bosons with couplings to nucleons conducted using a helioscope approach. No excess signal above background was found.

I. INTRODUCTION

The observed *CP* invariance in the strong interactions is not *a priori* expected, as 't Hooft pointed out [38], and has been named the *strong-CP problem*. Nonperturbative effects in the theory give rise to a *CP* violating term, " θ ", which appears in the QCD lagrangian as [29]

$$\mathcal{L}_\theta = \theta \frac{\alpha_S}{8\pi} F_{\mu\nu} \tilde{F}^{\mu\nu}. \quad (1)$$

Here, $F_{\mu\nu}$ is the gluon field strength and $\tilde{F}^{\mu\nu} =$

$\frac{1}{2}\epsilon_{\mu\nu\rho\sigma}F^{\rho\sigma}$ its dual. The apparent *CP* invariance of QCD derives from the fact that θ is measured to be vanishingly small via the neutron electric dipole moment, for which the current upper limit is $|d_n| < 6.3 \times 10^{-26} \text{ e cm}$ [18]. This limit on d_n implies an upper limit $\theta < 10^{-9}$ where $|d_n| = 5.2 \times 10^{-16}\theta \text{ e cm}$ [12].

In 1977, Peccei and Quinn proposed a physical origin for $\theta = 0$ by introducing a $U(1)$ symmetry [30], often referred to as $U(1)_{PQ}$. θ thus becomes a dynamical variable that is forced to zero when the potential is minimized. Weinberg showed that such a solution implies the existence of a new particle, the axion, and that such a particle can have couplings to quarks, nucleons, leptons and photons [40, 41].

In Sections IA, IB we briefly review the phenomenology of a pseudoscalar boson with couplings to photons and the origin of the hadronic axion. In Section II nuclear axion couplings are discussed and the signal expected from nuclear axion emission in the Sun from ${}^7\text{Li}$ (0.478 MeV) and $\text{D}(p, \gamma){}^3\text{He}$ (5.5 MeV) is described. In Sections III, IV the data selection, systematics, and anal-

*Corresponding author. Now at Stanford University; Electronic address: David.W.Miller@cern.ch

[†]Present address: Inst. de Physique Nucléaire, Lyon, France.

[‡]Present address: Department of Physics, Queen's University, Kingston, Ontario K7L 3N6, Canada

[§]Present address: Instituto de Física Nuclear y Altas Energías, Universidad de Zaragoza, Zaragoza, Spain

[¶]Permanent address: Brookhaven National Laboratory, NY-USA

ysis of the data are then presented in detail.

A. Axion-photon mixing

A common feature of all axion models, and of pseudoscalar bosons generally, is the two-photon interaction, or Primakoff effect [31]. We stress this generality because, as pointed out in [35], the phenomenology of the axion applies directly to pseudoscalar bosons in general.

In the Primakoff process an axion couples to a virtual photon in an EM field and converts to a real photon, or vice-versa. The conversion probability in a magnetic field of length L and strength B depends on the axion-photon coupling constant $g_{a\gamma}$ and the momentum transfer between the axion and the photon q as given in Eq. 2 [39]

$$P_{a \rightarrow \gamma}(L) = \frac{(g_{a\gamma} B/2)^2}{q^2 - \Gamma^2/4} \left(1 + e^{-\Gamma L} - 2e^{-\Gamma L/2} \cos(qL) \right) \quad (2)$$

where Γ is the inverse absorption length for the photons. For $qL \lesssim 1$ the probability of conversion reduces to $P_\gamma = (g_{a\gamma} B L/2)^2$ [37].

Axion-photon mixing permits a variety of production mechanisms and detection techniques, many of which were first pointed out by Sikivie in 1983 [37]. Magnetically induced vacuum birefringence [24], stellar and terrestrial magnetic fields, pulsar magnetic fields, and resonant cavities [37] all provide methods for the production or detection of axions. Experimental and astrophysical limits on the axion are typically stated in terms of the photon coupling, $g_{a\gamma}$, versus mass, m_a and recent experimental and cosmological limits are shown in Fig. 6 [33]

B. Hadronic axion model

The axion was first thought to have couplings on the order of the weak scale [40] and a mass of ~ 200 keV. Significant evidence against this coupling strength and mass range, most notably through limits on the magnetic moment of the muon, kaon decay and quarkonium studies, prompted Kim, Shifman, Vainshtein and Zakharov (KSVZ) to suggest the existence of an “invisible” axion [20, 36]. In this model, commonly referred to as the hadronic axion model, strong suppression of lepton couplings avoids many of the experimentally excluded properties of the Peccei-Quinn axion. Since couplings to nucleons and photons remain, detection of the hadronic axion is still possible. Other models have also been proposed with suppressed photon or nucleon couplings [13, 19] or which rely on the existence of different scalar fields from the KSVZ axion, but we focus here on axion models which include couplings to both photons and nucleons.

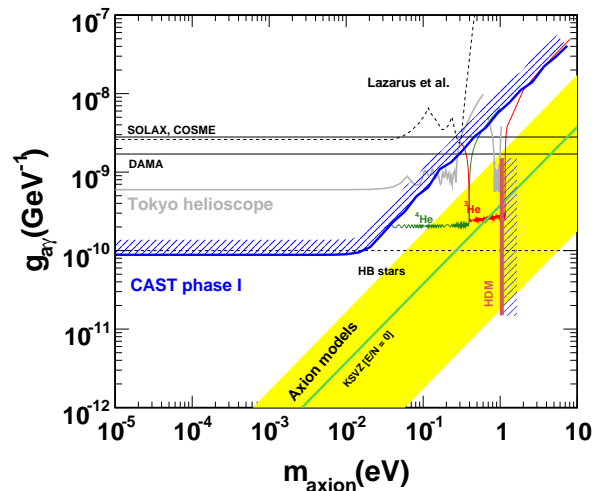


FIG. 1: Exclusion plots in the axion-photon coupling versus the axion mass plane. The limit achieved on Primakoff axions from the X-ray detectors by the previous Phase I of the CAST experiment [3] (updated limits consistent with expectations are reported in [4]) is compared with other constraints (Lazarus et al. [23], SOLAX [7], COSME [26], DAMA [10], Tokyo helioscope [27] and HB stars [32]). The vertical red line (HDM) is the hot dark matter limit for hadronic axions $m_a < 1.05$ eV [17] inferred from observations of the cosmological large-scale structure. The yellow band represents typical theoretical models with $|E/N - 1.95|$ in the range 0.07–7 while the green solid line corresponds to the case when $E/N = 0$ is assumed.

II. NUCLEAR AXION EMISSION IN HADRONIC AXION MODELS

A. Axion-nucleon coupling

Coupling to nucleons occurs through the spin operator σ [40] and because axions carry spin-parity $J^P = 0^-, 1^+, 2^-, \dots$ nuclear deexcitation via axion emission occurs predominantly via M1 magnetic nuclear transitions.

Several M1 nuclear transitions in the solar core provide channels for axion emission [21, 34], such as

$${}^7\text{*Li} \rightarrow {}^7\text{Li} + a(0.478\text{MeV}) \quad (3)$$

$$p + d \rightarrow \text{He}^3 + a(5.5\text{MeV}). \quad (4)$$

The ratio of axion-to-photon emission for such transitions depends on the axion mass and nucleon coupling strength and can be used to place limits on these parameters if the nucleon matrix elements and branching ratios are calculated (for example [6, 14, 21]).

The branching ratio for axion emission is directly calculated as [6, 19, 21, 28, 34]

$$\frac{\Gamma_a}{\Gamma_\gamma} = \frac{1}{2\pi\alpha} \left(\frac{k_a}{k_\gamma} \right)^3 \left(\frac{1}{1+\delta^2} \right) \times \left[\frac{g_0\beta + g_3}{(\mu_0 - 1/2)\beta + \mu_3 - \eta} \right]^2. \quad (5)$$

Here, k_a and k_γ are the axion and photon momenta, respectively, and will both be approximately equal to the decay channel energy. In addition, $\alpha = 1/137$, $\delta \sim 0$ is the $E2/M1$ mixing ratio, $\mu_0 \approx 0.88$ and $\mu_3 \approx 4.71$ are the isoscalar and isovector magnetic moments, respectively, which remain unchanged regardless of the nuclear transition responsible for the axion emission.

The remaining terms η and β are nuclear structure dependent parameters which depend directly on the initial and final state nuclear wavefunctions. It is via these terms that the *decay-channel specific* axion-physics enters the calculation, and they are given by

$$\eta = - \frac{\langle \mathbf{J}_f || \sum_{i=1}^A \mathbf{l}(i) \tau_3(i) || \mathbf{J}_i \rangle}{\langle \mathbf{J}_f || \sum_{i=1}^A \sigma(i) \tau_3(i) || \mathbf{J}_i \rangle}$$

$$\beta = \frac{\langle \mathbf{J}_f || \sum_{i=1}^A \sigma(i) || \mathbf{J}_i \rangle}{\langle \mathbf{J}_f || \sum_{i=1}^A \sigma(i) \tau_3(i) || \mathbf{J}_i \rangle}.$$

In Eq. (5) we have written the axion-nucleon coupling as $(g_0\beta + g_3)$, where g_0 is the isoscalar coupling and g_3 the isovector coupling. In the hadronic axion models these are written as [19]

$$\begin{aligned} g_0 &= -\frac{m_N}{f_a} \frac{1}{6} \left[2S + (3F - D) \frac{1+z-2w}{1+z+w} \right] \\ g_3 &= -\frac{m_N}{f_a} \frac{1}{2} \left[(D + F) \frac{1-z}{1+z+w} \right] \end{aligned} \quad (6)$$

where f_a is the Peccei-Quinn axion energy scale, $S = 0.4$ characterizes the flavor singlet coupling, $F = 0.460$ and $D = 0.806$ are matrix elements for the SU(3) octet axial vector currents, $z = m_u/m_d = 0.56$ and $w = m_u/m_s = 0.028$ are the quark mass ratios, and $m_N = 0.939$ GeV is the nucleon mass, yielding $g_0 = 2.10 \times 10^{-7}$ and $g_3 = 1.65 \times 10^{-7}$.

B. Expected axion flux from ${}^7\text{Li}^* \rightarrow {}^7\text{Li} + a$

The decay of the first excited state of ${}^7\text{Li}$

$${}^7\text{Li}^* \rightarrow {}^7\text{Li} + \gamma(0.478\text{MeV}), \quad (7)$$

follows ${}^7\text{Be}$ electron capture and can emit an axion of the same kinetic energy instead of a γ -ray. Following the

work of [6, 21] we can write $d\Phi_a/dE_a$, the flux of axions arriving at Earth, as

$$\begin{aligned} \frac{d\Phi_a}{dE_a} &= \int_0^{R_\odot} d\Phi_\nu^{Be}(r) \kappa \frac{\Gamma_a}{\Gamma_\gamma} \frac{1}{\sqrt{2\pi}\sigma(T)} \\ &\times \exp \left[-\frac{(E_a - E_\gamma)^2}{2\sigma(T)^2} \right], \end{aligned} \quad (8)$$

where R_\odot is the solar radius, $d\Phi_\nu^{Be}(r)$ is the ${}^7\text{Be}$ neutrino flux at Earth emitted from a solar shell at radius r , $\kappa = 0.104$ is the branching ratio of the ${}^7\text{Be}$ electron capture to the first excited state [16], $\sigma(T) = E_\gamma \sqrt{kT}/m$ is a Doppler broadening of the emission line due to thermal motion of the nuclei in the sun, and Γ_a/Γ_γ is the axion-photon branching ratio.

In [21], $\eta = 0.5$ and $\beta = 1.0$ are calculated based on shell model estimations, and we will use these values here, obtaining

$$\frac{\Gamma_a}{\Gamma_\gamma} = 1.035(g_0\beta + g_3)^2 \text{ cm}^{-2}\text{sec}^{-1}. \quad (9)$$

Since the resolution of the calorimeter (σ_{det}) in the energy region around 450 keV is $\sigma_{det} \approx 21\% \approx 100$ keV, we integrate over the Doppler broadening term and use the total neutrino flux at Earth $\Phi_\nu^{Be} = 4.86 \times 10^9 \text{ cm}^{-2} \text{ sec}^{-1}$ [8]. Thus, we wash out the Doppler term and obtain only a factor of 1/2, such that

$$\Phi_a = 2.615 \times 10^8 (g_0\beta + g_3)^2 \text{ cm}^{-2}\text{sec}^{-1}. \quad (10)$$

It is interesting to note the relative insensitivity of Φ_a to the choice of η and β above. By varying $0.1 \leq \eta \leq 0.9$ and $0.6 \leq \beta \leq 1.4$, Φ_a varies between $1.612 \times 10^8 \leq \Phi_a/(g_0\beta + g_3)^2 \leq 4.397 \times 10^8$ (in this range of η and β). Thus, the more critical parameter is the emission rate, which for ${}^7\text{Li}$ follows the ${}^7\text{Be}$ neutrinos, Φ_ν^{Be} .

C. Expected axion flux from $D(p, \gamma){}^3\text{He}$

Also of interest for hadronic axions is the radiative capture of protons on deuterium, also referred to as proton-deuteron fusion [34]. The reaction

$$p + d \rightarrow {}^3\text{He} + \gamma \quad (11)$$

occurs $1.7 \times 10^{38} \text{ sec}^{-1}$ [34] with only 1/3 of those being M1 transitions. In order to obtain the axion flux expected from (11) we must evaluate Eq. (5) using the correct η and β , which is made difficult by the fact that (11) is a 3-body nuclear decay. However, as pointed out by [34], (11) is predominantly isovector, implying that $g_0\beta$ is very small and can be neglected. Under this assumption, Eq. (5) becomes

$$\frac{\Gamma_a}{\Gamma_\gamma} = \frac{1}{2\pi\alpha} \left(\frac{k_a}{k_\gamma} \right)^3 \left(\frac{1}{1+\delta^2} \right) \left[\frac{g_3}{\mu_3} \right]^2. \quad (12)$$

Using $\delta=0$, $k_a \approx k_\gamma = 5.5$ MeV, and $\mu_3 = 4.71$ we have for (11)

$$\frac{\Gamma_a}{\Gamma_\gamma} = 0.98 g_3^2. \quad (13)$$

Combining Eqs.(6,13) yields

$$\begin{aligned} \Phi_a &= \frac{\Phi_\gamma g_3^2}{12\pi d_\odot^2} \\ &= 2.03 \times 10^{10} g_3^2 \text{ cm}^{-2} \text{ sec}^{-1}. \end{aligned} \quad (14)$$

Using the data obtained from the 6 month run in 2006, we can thus evaluate the sensitivity of the CAST γ -ray calorimeter to these axion signals.

III. DATA

A. CAST and the high energy γ calorimeter

The CERN axion solar telescope (CAST) utilizes a helioscope design which exploits the increased axion-to-photon conversion probability for increased magnetic field strength and length (see Eq. 2 below). The refurbished LHC dipole prototype magnet [43] produces a nominal magnetic field of $B = 9.0$ T over a length of $L = 9.26$ m in each of the dipole's two 14.5 cm^2 area magnet bores. The full system is mounted on a rotating platform with a vertical range of $\pm 8^\circ$ and an azimuthal range of $\pm 40^\circ$. This range of motion allows for 1.5 hours of solar alignment during both sunrise and sunset, as well as year round solar tracking. The tracking system software monitors the alignment of the magnet, resulting in a pointing accuracy better than 0.01° . All remaining time is devoted to background measurements for the three low-background X-ray detectors: a Time Projection Chamber (TPC) [5], micro mesh gas detector referred to as a MICROMEAS [22], and a solid state X-Ray CCD camera coupled to a X-Ray telescope used to increase signal to noise [2]. During the second year of Phase I data-taking, the low-background γ -ray calorimeter was installed behind the MICROMEAS detector (which is transparent to the photon energies of interest) to perform a parasitic search for high-energy axions (see Fig. 2(a)).

Axions emitted in nuclear processes will be mono-energetic compared to the Primakoff spectrum expected from plasma processes and have kinetic energies from tens of keV to many MeV. The expected axion signal is thus a collimated beam of similarly mono-energetic γ -rays from the magnet bore during periods of solar alignment.

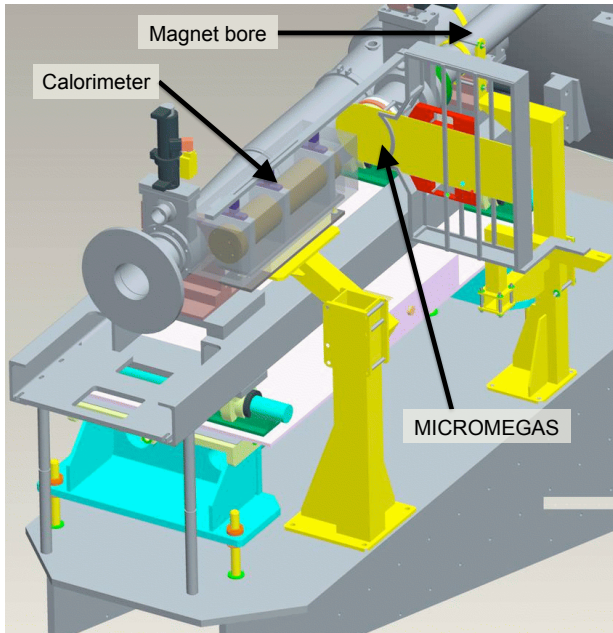
The calorimeter consists of a cadmium tungstate scintillating crystal (CdWO_4 or CWO), which is also the type used in neutrinoless double-beta decay searches [15]. CWO offers good stopping power for γ -ray photons, very low internal radioactivity, good energy resolution and excellent pulse shape discrimination characteristics (see Section III B). The crystal is optically coupled to a light guide and photomultiplier tube (PMT) which is placed inside a lead-shielded cylindrical brass tube. This “tunnel” design maximizes signal acceptance and background rejection while respecting the space and weight limitations on the CAST detector platform (see Fig. 2(b)). The modest thickness (2.5 cm) of ancient and common lead shielding results in an elevated environmental background component compared to that achievable with fewer constraints. An active scintillating plastic muon veto, environmental radon purging with constant N_2 flow, a borated thermal neutron absorber, and a low-background PMT complement the minimalist passive shielding design.

The large dynamic range and high stopping power for photons are necessary to achieve a good efficiency at high energies for a general high-energy search. Detector components, shielding materials, and data processing were all designed in order to reduce the environmental backgrounds. Pulse shape discrimination (PSD) further reduces noise and events due to internal radioactive contaminations in the crystal. Finally, an LED pulser provides livetime monitoring. These square pulses are recorded and subsequently removed prior to analysis.

Although similar searches have been conducted in beam dump experiments [11, 42], accelerators and terrestrial nuclear processes [21, 25], CAST is the first high-energy-axion search using a helioscope. The order of magnitude increase in conversion probability over previous helioscope searches and the increase in the intensity of axion emission as compared to accelerator searches makes the CAST calorimeter a very sensitive probe of low-mass pseudoscalars. Because axions serve as a one example of such particles, a high-energy search should not be limited to only axions but should consider anomalous excess during solar tracking events generally [32, 35].

B. Event selection and cuts

Following a method similar to [15], we developed and applied a pulse shape discrimination (PSD) algorithm which exploits the distinct pulse shape characteristics of the CWO crystal in response to incident particle type. The PSD algorithm is applied to the data to remove backgrounds and noise. By using both *in situ* γ calibrations and previous laboratory tests, event selection criteria are set before being applied to acquired data and remain consistent throughout the analysis. These criteria are first set using γ calibration data to maintain a calibration signal acceptance of 99.7%, while rejecting 100% of the noise and square pulses from the livetime pulser. Discrimina-



(a) CAST magnet platform

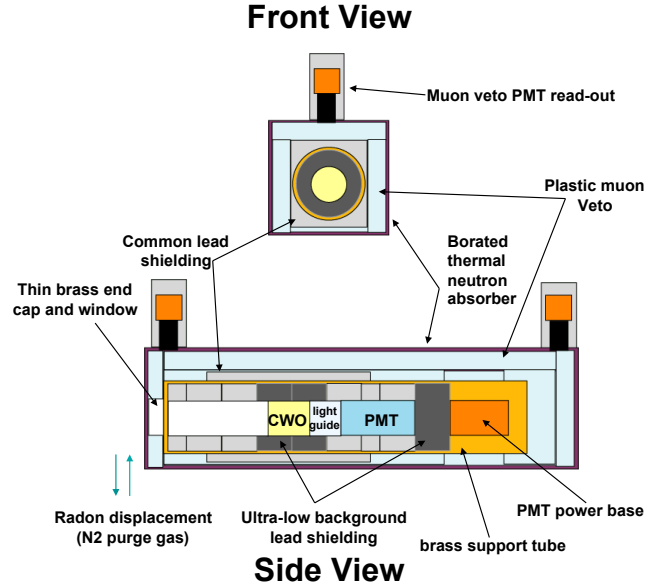
(b) CAST high energy γ -ray calorimeter

FIG. 2: (a) Schematic of the CAST magnet platform depicting the calorimeter placement behind the MICROMEGAS detector and the space constraints limiting the allowed shielding. (b) Schematic of the CAST high energy γ -ray calorimeter. The “tunnel” design with CWO crystal and PMT surrounded by modest amount of ancient and common lead passive shield. An active muon veto with dual PMT read-out, borated neutron absorber and continuous N_2 radon purging complement the passive shielding.

tion against α 's and n 's is not overly aggressive and the cuts have been placed at approximately the 3σ signal acceptance level for low energies. This yields a background α rejection of $\sim 50\%$. Due to the difficulties in obtaining the optimal algorithm for neutron rejection, the neutron rejection capability has not been fully quantified for this analysis. The exact fraction of neutron recoils rejected would be exactly characterized with the help of a pure, mono-energetic neutron emitter which was not available at the time of the calorimeter commissioning and operation.

C. Solar tracking and background data

Both background and tracking events are considered for analysis using the same run condition criteria, while solar tracking events have the further requirement that the magnet be sufficiently aligned with the solar core. Corrections are then applied to correct for a small background energy spectrum dependence on the pointing position of the CAST magnet, due to differences in natural radioactive background changes throughout the CAST experimental hall. Following these corrections, the background and tracking (signal) data sets can be reliably compared.

The dataset from the 2004 run includes a total of 1257 hours of total exposure time with 60.2 hours of solar

Total exposure time	1257.06 hrs
Solar tracking	60.256 hrs
Background	897.835 hrs
Normalized background	117.34 hrs
BCKG rate after cuts	1.429 Hz
BCKG flux (above 200 MeV)	$0.1 \text{ cm}^{-2} \text{ s}^{-1}$

TABLE I: Statistics of the data set used in this analysis.

alignment, 897.8 hours of background data and 117 hours of effective background data after normalization to position. A summary of the statistics for this data set is shown in Table I. Following the position normalization, the effective background data set still consists of roughly $2\times$ the tracking data, thus maintaining good statistics for background subtraction.

To facilitate the analysis over such a large dynamic range, the data have been divided into three energy regions (0.2-3.0 MeV, 3.0-10 MeV, 10-100 MeV) and binned according to the detector resolution in each region. The energy spectra for both tracking and background in each energy range are shown in Figs. 3. Environmental γ radioactivity is very evident in the low energy region. γ 's from ambient ^{40}K activity (1.460 MeV) and ^{208}Tl (2.614 MeV) from the ^{232}Th decay chain exhibit prominent peaks in the data, along with e^+e^- annihilation γ 's at 0.511 MeV.

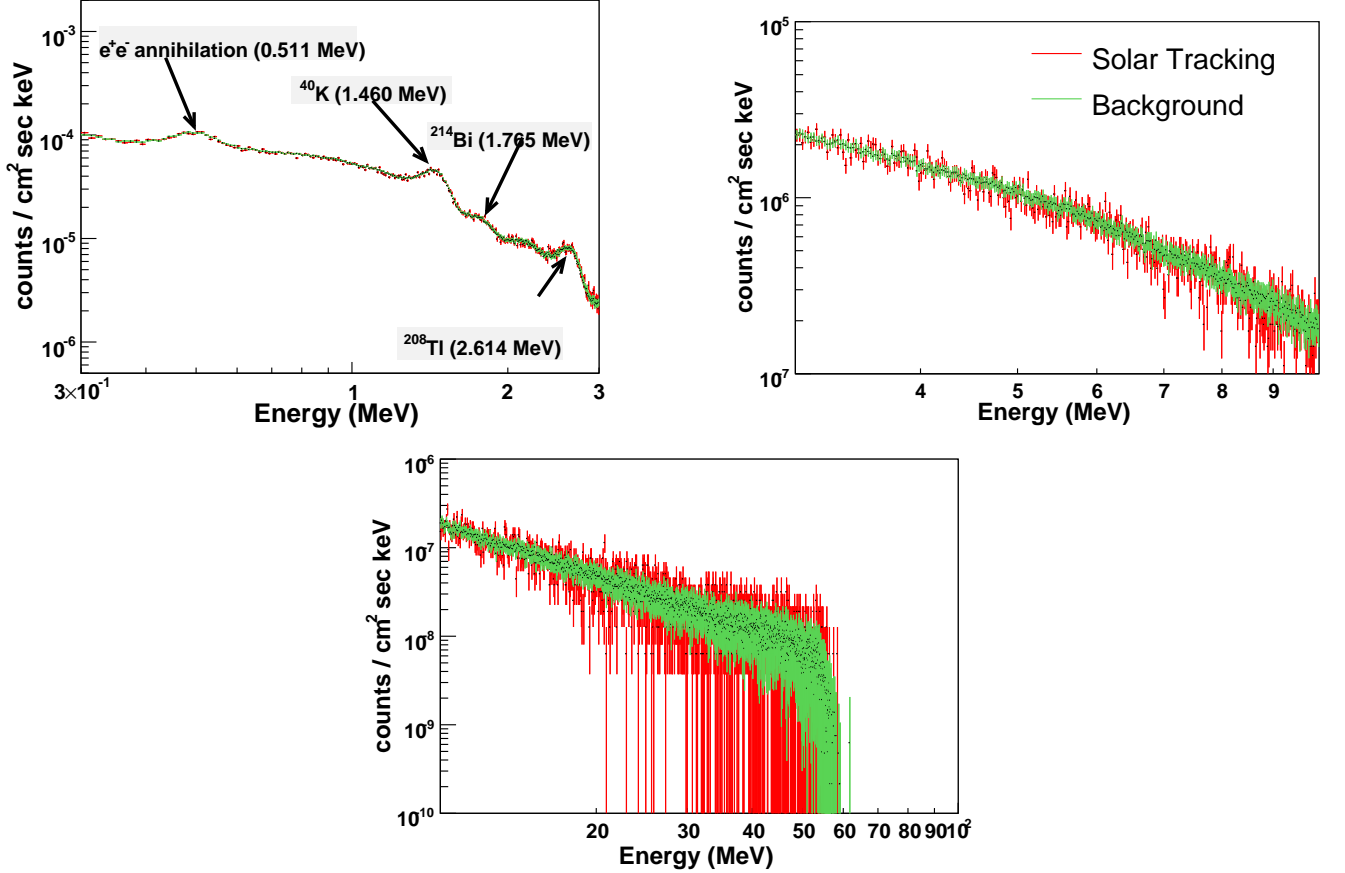


FIG. 3: Tracking and background energy spectra for each energy region in the analysis. The background spectra used have been normalized to the time and position of the tracking data and PSD and energy cuts have been applied. Prominent in the low energy region are decays from ^{40}K activity (1.460 MeV), ^{208}Tl (2.614 MeV) from the ^{232}Th decay chain, ^{214}Bi (1.76 MeV) from the ^{238}U decay chain, and e^+e^- annihilation γ 's at 0.511 MeV.

IV. DATA ANALYSIS AND LIMITS ON AXION EMISSION FROM ^7Li AND $\text{D}(p, \gamma)^3\text{He}$

A. Expected axion signal

Direct background subtraction from the tracking data permits the search for excess events in the residual energy spectrum. The expected signal from axion-photon conversion is a collimated “beam” of mono-energetic photons from the magnet bore during times of solar alignment. This results in Gaussian energy depositions in the CWO crystal for low energy (below 1.022 MeV) photons.

Above 1.022 MeV, an axion conversion photon may pair-produce within the crystal. For each pair-production, there is a possibility that one or both photons escape. These annihilation escape peaks will lie at 0.511 and 1.022 MeV below the full energy peak and the efficiency for catching these events is characteristic of both the crystal and the energy of the incident axion-conversion photon.

An MCNP4b [1] simulation of this spectrum for a 5.5

MeV photon, convolved with the detector resolution, is used to determine calorimeter sensitivity to photons at this energy. Photon detection efficiency is nearly 55% when considering the entire range at 5.5 MeV for this signal. The multi-peak signal shape and increased photon detection efficiency thus improves the sensitivity to excess events above 4.0 MeV. A general search along the entire energy spectrum of the calorimeter would require a full Monte Carlo analysis of the signal shape and its energy dependence. Here, only a 5.5 MeV photon signal has been investigated using this approach, while at all other energies below 10 MeV only a single Gaussian signal (corresponding to a full energy peak) is used. The 5.5 MeV signal is fit as two Gaussians, to a good approximation, which have a fixed peak-height ratio given by the simulation. The 95% CL for the number of allowed counts for such a signal is 2.14×10^{-5} counts $\text{cm}^{-2}\text{s}^{-1}$, or 4.51×10^{-5} γ 's $\text{cm}^{-2}\text{s}^{-1}$ when including the livetime of the detector and the detection efficiency.

Above 10 MeV, photonuclear dissociation is both energetically possible and very probable, with cross sections

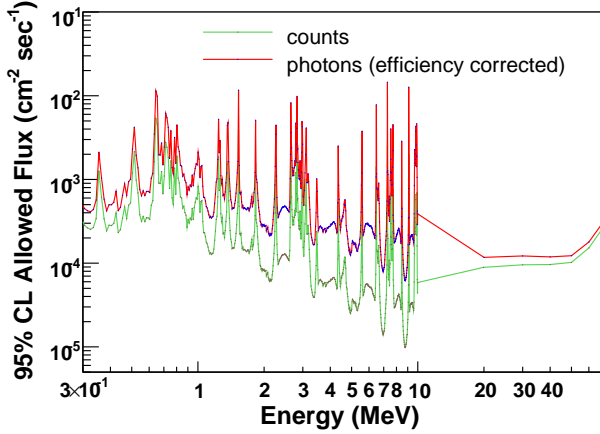


FIG. 4: 95% CL limits on the number of counts above background yield limits on the flux of axion-conversion photons incident on the CAST calorimeter after correcting for detection efficiency and livetime. These limits may then be directly translated into the allowed flux of axions incident on the helioscope. Below 10 MeV, a Gaussian energy deposition signal is used. At higher energies, the photonuclear cross section alters the energy deposition signal and the analysis is performed for 20, 30, 40, 50, 60 and 70 MeV.

for interaction near 1 barn for the tungsten and cadmium in the CWO crystal. This large cross section for photonuclear dissociation results in a much different energy deposition shape in the CWO crystal than for low energy photons and so the shape of the deposition signal can no longer be approximated by a Gaussian. In this energy regime, the total energy deposition efficiency is determined via MCNP4b simulation and depends very heavily on the cross-section for photonuclear interactions above 10 MeV.

B. Allowed anomalous events

We perform a general search for excess events across the entire dynamic range of the detector by fitting the known spectral shape to the residual energy spectrum remaining after background subtraction. For the analysis presented here, a Gaussian energy deposition has been used below 10 MeV with the exception of the 5.5 MeV photon signal, as stated in Section IV A.

The results of the 95% CL fits of a (Gaussian + background) energy deposition signal to the entire energy range of the detector are shown in Fig. 4. The structure present in the plot is a general consequence of statistical fluctuations in the residual spectrum of the data which lead to large or small 95% CL bounds on the Gaussian and are physically meaningful as they can point to incomplete subtraction or to slight statistical excesses in the data.

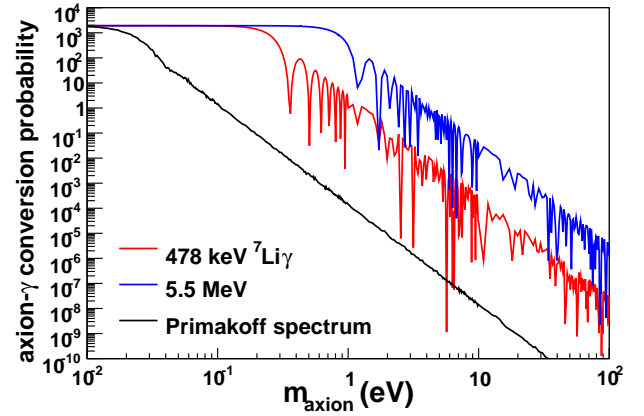


FIG. 5: The enhancement of the axion- γ conversion probability is due to the higher axion kinetic energy in nuclear emission processes. Axions from ${}^7\text{Li}$ decay (478 keV) and p-d fusion (5.5 MeV) show 4 and 6 orders of magnitude improvement, respectively, in axion-photon conversion for a given $g_{a\gamma}$ and m_a .

C. Calorimeter sensitivity to ${}^7\text{Li}^* \rightarrow {}^7\text{Li} + a$

In order to evaluate the detector sensitivity to axion emission from specific decay channels, several parameters are included and are found in Table II.

Parameter		Value
Peak efficiency	Ω_{peak}	57% combined
Photon transm. efficiency	Ω_{transm}	
Livetime	τ_{det}	93%
Software cuts efficiency	Ω_{cuts}	99%
Conversion probability	$P_{a \rightarrow \gamma}$	(see Fig. 5)

TABLE II: Calorimeter characteristics.

From MCNP Monte Carlo simulations, at the energy of the ${}^7\text{Li}$ decay, 478 keV, the efficiency for peak energy deposition is 57%. Including all known detector inefficiency, Ω_{total} , we can estimate the sensitivity to axions from ${}^7\text{Li}$ decays using

$$\begin{aligned} \Phi_{478 \text{ keV}} &= P_{a \rightarrow \gamma}(m_a) \Phi_a \tau_{det} \Omega_{total} \\ &= 1.373 \times 10^8 P'_{a \rightarrow \gamma}(m_a) \\ &\quad \times g_{a\gamma}^2 (g_0 \beta + g_3)^2 \text{ cm}^{-2} \text{ sec}^{-1} \end{aligned} \quad (15)$$

Here we have separated the conversion probability $P_{a \rightarrow \gamma}$ into its numerical part $P'_{a \rightarrow \gamma}(m_a)$, that only depends on the magnet parameters and the axion kinetic energy and mass, and the axion- γ coupling constant $g_{a\gamma}$. $P'_{a \rightarrow \gamma}(m_a)$ versus m_a is shown in Fig. 5.

The limit on anomalous events at 478 keV is $\Phi_{478 \text{ keV}}(95\% \text{CL}) \leq 3 \times 10^{-4} \text{ cm}^{-2} \text{ sec}^{-1}$ (see Fig. 4). By solving for $g_{a\gamma}$ in Eq. (15) we can write

$$g_{a\gamma} \leq \frac{1}{g_0 \beta + g_3} \sqrt{\frac{\Phi_{478 \text{ keV}}(95\% \text{CL})}{1.373 \times 10^8} \frac{1}{P'_{a \rightarrow \gamma}}} \quad (16)$$

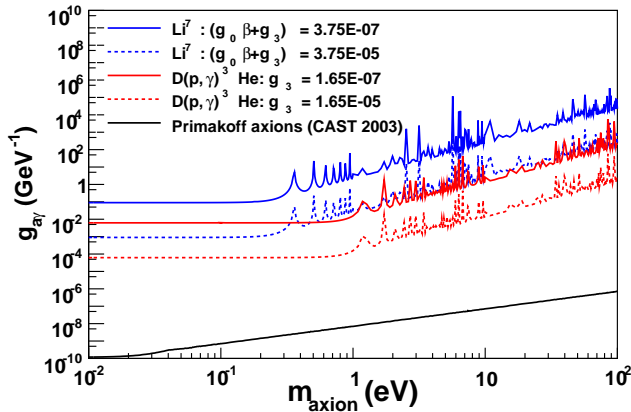


FIG. 6: The limits obtained on the axion-photon coupling versus axion rest mass for 478 keV axions from ${}^7\text{Li}$ decay and 5.5 MeV axions from proton-deuteron fusion for two values of the nuclear couplings. This parasitic axion search has not found any evidence for new pseudoscalar particles coupling to nucleons.

The limits obtained from Eq. (16) as a function of m_{axion} are shown in Fig. 6.

D. Calorimeter sensitivity to $\text{D}(p, \gamma)^3\text{He}$

Using again the information from Table II, we can evaluate the limiting expression for $g_{a\gamma}$ as

$$\Phi_{5.5 \text{ MeV}} = 1.065 \times 10^{10} P'_{a \rightarrow \gamma}(m_{axion}) \times g_{a\gamma}^2 g_3^2 \text{ cm}^{-2} \text{ sec}^{-1} \quad (17)$$

For (11), the expected signal differs from that of ${}^7\text{Li}$ since a 5.5 MeV γ -ray can pair-produce within the calorimeter. This escape peak structure has been taken into account and the 95% CL limit on anomalous counts is $\Phi_{5.5 \text{ MeV}}(95\% \text{CL}) \leq 2.14 \times 10^{-5} \text{ events cm}^{-1} \text{ sec}^{-1}$. Using Eq. 17 we have

$$g_{a\gamma} \leq \frac{1}{g_3} \sqrt{\frac{\Phi_{5.5 \text{ MeV}}(95\% \text{CL})}{1.065 \times 10^{10}} \frac{1}{P'_{a \rightarrow \gamma}}} \quad (18)$$

By plotting Eq. (18) against axion mass, we again see

that are weaker than those obtained by the CAST X-ray detectors in 2003.

This direct helioscope search for axions from nuclear de-excitation, as in (7), is the first of its kind, and provides an important cross-check for other searches focused on nuclear decay, such as [9, 21]. Furthermore, as discussed in [34], the search for axions from (4) is much more general than Primakoff axions or KSVZ axions since (4) is both M1 and E1 and can couple to particles of various spin-parity.

V. CONCLUSIONS

The CAST photon calorimeter provides a model independent search for high-energy axion-photon conversions during period of solar alignment. This is the first such search for high-energy pseudoscalar bosons with couplings to nucleons conducted using a helioscope approach. The parasitic nature of this search, making use of the CAST magnet, limits the sensitivity achievable. A dedicated high-energy axion search performed underground and without shielding limitations would be able to reach background levels many orders of magnitude lower and is necessary to reach the very small axion flux expected from the two axion emission channels considered in this search. CAST remains a unique instrument allowing for serendipitous searches for anomalous solar emissions in the form of new particles with coupling to photons with unprecedented sensitivity.

VI. ACKNOWLEDGEMENTS

We would like to thank the entire CAST collaboration and CERN for making this experiment possible. We acknowledge support from NSERC (Canada), MSES (Croatia) under the grant number 098-0982887-2872, CEA (France), BMBF (Germany) under the grant numbers 05 CC2EEA/9 and 05 CC1RD1/0, the Virtuelles Institut für Dunkle Materie und Neutrinos – VIDMAN (Germany), GSRT (Greece), RFFR (Russia), CICyT (Spain), NSF (USA), US Department of Energy, NASA under the grant number NAG5-10842 and the helpful discussions within the network on direct dark matter detection of the ILIAS integrating activity (Contract number: RII3-CT-2003-506222).

-
- [1] *MCNP, A General Monte Carlo N-Particle Transport Code*.
 [2] P. Abbon, S. Andriamonje, S. Aune, T. Dafni, M. Davenport, E. Delagnes, R. de Oliveira, G. Fanourakis, E. Ferrer Ribas, J. Franz, T. Geralis, A. Giganon, M. Gros, Y. Giomataris, I. G. Irastorza, K. Kousouris, J. Morales, T. Papaevangelou, J. Ruz, K. Zachariadou, and K. Zioutas. The micromegas detector of the cast

- experiment. *New J. Phys.*, 9:170–+, June 2007.
 [3] S. Andriamonje et al. An improved limit on the axion-photon coupling from the cast experiment. *JCAP*, 0704:010, 2007.
 [4] E. Arik, S. Aune, D. Autiero, K. Barth, A. Belov, B. Beltran, S. Borghi, G. Bourlis, F.S. Boydag, H. Brauningner, J.M. Carmona, S. Cebrian, S.A. Cetin, J.I. Collar, T. Dafni, M. Davenport, L. Di Lella, O.B. Dogan,

- C. Eleftheriadis, N. Elias, G. Fanourakis, E. Ferrer-Ribas, H. Fischer, P. Friedrich, J. Franz, J. Galan, T. Geralis, I. Giomataris, S. Gninenko, H. Gomez, R. Hartmann, M. Hasinoff, F.H. Heinsius, I. Hikmet, D.H.H. Hoffmann, I.G. Irastorza, J. Jacoby, K. Jakovcic, D. Kang, K. Konigsmann, R. Kotthaus, M. Krcmar, K. Kousouris, M. Kuster, B. Lakic, C. Lasseur, A. Liolios, A. Ljubicic, G. Lutz, G. Luzon, D. Miller, J. Morales, T. Niinikoski, A. Nordt, A. Ortiz, T. Papaevangelou, M.J. Pivovarov, A. Placci, G. Raffelt, H. Riege, A. Rodriguez, J. Ruz, I. Savvidis, Y. Semertzidis, P. Serpico, R. Soufli, L. Stewart, K. van Bibber, J. Villar, J. Vogel, L. Walckiers, and K. Zioutas. Probing eV-scale axions with cast. *Journal of Cosmology and Astroparticle Physics*, 2009(02):008, 2009.
- [5] D. Autiero, B. Beltrán, J. M. Carmona, S. Cebrián, E. Chesi, M. Davenport, M. Delattre, L. Di Lella, F. Formenti, I. G. Irastorza, H. Gómez, M. Hasinoff, B. Lakić, G. Luzón, J. Morales, L. Musa, A. Ortiz, A. Placci, A. Rodríguez, J. Ruz, J. A. Villar, and K. Zioutas. The cast time projection chamber. *New J. Phys.*, 9:171–+, June 2007.
- [6] F. T. III. Avignone, C. Baktash, W. C. Barker, F. P. Calaprice, R. W. Dunford, W. C. Haxton, R. T. Kahana, D. Kouzes, H. S. Miley, and D. M. Moltz. Search for axions from the 1115-keV transition of ^{65}Cu . *Phys. Rev. D*, 37:618–630, 1988.
- [7] F. T. III. Avignone and *et al* (SOLAX Collaboration). Experimental search for solar axions via coherent Primakoff conversion in a germanium spectrometer. *Phys. Rev. Lett.*, 81:5068, 1998.
- [8] J. N. Bachall and M. H. Pinsonneault. What Do We (Not) Know Theoretically about Solar Neutrino Fluxes? *Phys. Rev. Lett.*, 92:121301, 2004.
- [9] G. Bellini and *et al*. Search for solar axions emitted in the M1-transition of $^7\text{Li}^*$ with Borexino CTF. *European Physical Journal C*, 54:61–72, 2008.
- [10] R. Bernabei and *et al*. Search for solar axions by Primakoff effect in NaI crystals. *Phys. Lett. B*, 515:6, 2001.
- [11] J. D. Bjorken, S. Ecklund, W. R. Nelson, A. Abashian, C. Church, B. Lu, T. A. Mo, L. W. Nunamaker, and P. Rassmann. Search for neutral metastable penetrating particles produced in the SLAC beam dump. *Phys. Rev. D*, 38:3375–3386, 1988.
- [12] R. J. Crewther, P. di Vecchia, G. Veneziano, and E. Witten. Chiral estimate of the electric dipole moment of the neutron in quantum chromodynamics. *Phys. Lett. B*, 88:123–127, December 1979.
- [13] M. Dine, W. Fischler, and M. Srednicki. A simple solution to the strong CP problem with a harmless axion. *Phys. Lett. B*, 104:199–202, 1981.
- [14] T. W. Donnelly, S. J. Freedman, R. S. Lytel, R. D. Peccei, and M. Schwartz. Do axions exists? *Phys. Rev. D*, 18:1607–1620, 1978.
- [15] T. Fazzini, P. G. Bizzeti, P. R. Maurenzig, C. Stramaccioni, F. A. Danevich, V. V. Kobaychev, V. I. Tretyak, and Yu. G. Zdesenko. Pulse shape discrimination with CdWO_4 crystal scintillators. *Nuclear Instruments and Methods in Research A*, 410:213–219, 1997.
- [16] R. B. Firestone, editor. *Table of Isotopes*. Wiley Interscience, 1996.
- [17] S. Hannestad, A. Mirizzi, and G. Raffelt. A new cosmological mass limit on thermal relic axions. *Journal of Cosmology and Astroparticle Physics*, page 002, 2005.
- [18] P. G. Harris, C. A. Baker, K. Green, P. Iaydjiev, S. Ivanov, D. J. R. May, J. M. Pendlebury, D. Shiers, K. F. Smith, M. van der Grinten, and P. Geltenbort. New experimental limit on the electric dipole moment of the neutron. *Phys. Rev. Lett.*, 82:904–907, 1999.
- [19] D. B. Kaplan. Opening the Axion Window. *Nuclear Physics B*, 260:215–226, 1985.
- [20] J. K. Kim. Weak-interaction singlet and strong CP invariance. *Phys. Rev. Lett.*, 2:103–107, 43.
- [21] M. Krčmar, Z. Krečak, A. Ljubičić, M. Stipčević, and D. A. Bradley. Search for solar axions using ^7Li . *Phys. Rev. D*, 64:115016, November 2001.
- [22] M. Kuster, H. Bräuninger, S. Cebrián, M. Davenport, C. Eleftheriadis, J. Englhauser, H. Fischer, J. Franz, P. Friedrich, R. Hartmann, F. H. Heinsius, D. H. H. Hoffmann, G. Hoffmeister, J. N. Joux, D. Kang, K. Königsmann, R. Kotthaus, T. Papaevangelou, C. Lasseur, A. Lippitsch, G. Lutz, J. Morales, A. Rodríguez, L. Strüder, J. Vogel, and Zioutas. The x-ray telescope of cast. *New J. Phys.*, 9:169–+, June 2007.
- [23] D. M. Lazarus, G. C. Smith, R. Cameron, A. C. Melissinos, G. Ruoso, Y. K. Semertzidis, and F. A. Nezrick. Search for Solar Axions. *Phys. Rev. Lett.*, 69:2333–2336, 1992.
- [24] L. Maiani, R. Petronzio, and E. Zavattini. Search for axions in specific nuclear gamma transitions as a power reactor. *Phys. Lett. B*, 110:359–363, August 1982.
- [25] M. Minowa, Y. Inoue, T. Asanuma, and M. Imamura. Invisible axion search in ^{139}La M1 transition. *Phys. Rev. Lett.*, 71:4120–4123, 1993.
- [26] A. Morales and *et al* (COSME Collaboration). Particle dark matter and solar axion searches with a small germanium detector at the Canfranc underground laboratory. *Astropart. Phys.*, 16:325, 2002.
- [27] S. Moriyama, M. Minowa, T. Namba, Y. Inoue, Y. Takasu, and A. Yamamoto. Direct search for solar axions by using strong magnetic field and x-ray detectors. *Phys. Lett. B*, 434:147–152, 1998.
- [28] T. Moroi and H. Murayama. Axionic hot dark matter in the hadronic axion window. *Phys. Lett. B*, 440:69–76, 1998.
- [29] H. Murayama. Axions and other very light bosons. *Phys. Lett. B*, 592:389–391, 2004.
- [30] R. D. Peccei and H. R. Quinn. CP Conservation in the Presence of Pseudoparticles. *Phys. Rev. Lett.*, 38:1440–1443, June 1977.
- [31] H. Primakoff. Photo-Production of Neutral Mesons in Nuclear Electric Fields and the Mean Life of the Neutral Meson. *Phys. Rev.*, 81:899, 1951.
- [32] G. Raffelt. Stars as Laboratories for Fundamental Physics. *University of Chicago Press*, 1996.
- [33] G. Raffelt. Stars and Fundamental Physics. *hep-ph/*, 0207144, 2002.
- [34] G. Raffelt and L. Stodolsky. New Particles from Nuclear Reactions in the Sun. *Phys. Lett. B*, 119:323, 1982.
- [35] G. Raffelt and L. Stodolsky. Mixing of the photon with low-mass particles. *Phys. Rev. D*, 37:1237–1249, 1988.
- [36] M. A. Shifman, A. I. Vainshtein, and V. I. Zakharov. Can confinement ensure natural CP invariance of the strong interactions? *nucpb*, 166:493–506, 1980.
- [37] P. Sikivie. Experimental Tests of the “Invisible” Axion. *Phys. Rev. Lett.*, 51:1415–1417, 1986.
- [38] G. ’t Hooft. Symmetry breaking through Bell-Jackiw

- anomalies. *Phys. Rev. Lett.*, 37:8–11, 1976.
- [39] K. van Bibber, P. M. MacIntyre, D. E. Morris, and G. G. Raffelt. Design for a practical laboratory detector for solar axions. *Phys. Rev. D*, 39:2089–2099, 1989.
 - [40] S. Weinberg. A New Light Boson? *Phys. Rev. Lett.*, 40:223–226, January 1978.
 - [41] F. Wilczek. Problem of Strong P and T Invariance in the Presence of Instantons. *Phys. Rev. Lett.*, 40:279–282, January 1978.
 - [42] A. Zehnder, K. Gabathuler, and J. L. Vuilleumier. Search for axions in specific nuclear gamma transitions as a power reactor. *Phys. Lett. B*, 110:419–422, 1982.
 - [43] K. et al Zioutas. A Decommissioned LHC Model Magnet as an Axion Telescope. *Nuclear Instruments and Methods in Research A*, 425:480–487, 1999.